Title: Rapid thinning of Pine Island Glacier in the early Holocene

Authors: J. S. Johnson[1]*†, M. J. Bentley[2,1]†, J. A. Smith[1], R. C. Finkel[3,4], D. H. Rood[3,5]‡, K. Gohl[6], G. Balco[7], R. D. Larter[1], J. M. Schaefer[8,9]

Affiliations:

[1]British Antarctic Survey, Natural Environment Research Council, High Cross, Madingley Road, Cambridge, CB3 0ET, United Kingdom

[2]Durham University, South Road, Durham, DH1 3LE, United Kingdom

[3]Center for Accelerator Mass Spectrometry, Lawrence Livermore National Laboratory, P.O. Box 808 L-397, Livermore, CA 94550, USA

[4]Earth and Planetary Science Department, University of California, Berkeley, CA 94720, USA

[5]Earth Research Institute, University of California, Santa Barbara, CA 93106, USA

[6]Alfred Wegener Institute Helmholtz-Centre for Polar and Marine Research, Am Alten Hafen 26, 27568 Bremerhaven, Germany.

[7]Berkeley Geochronology Center, 2455 Ridge Road, Berkeley, CA 94709, USA

[8]Lamont-Doherty Earth Observatory, Columbia University, Route 9W, Palisades, NY 10964, USA

[9]Department of Earth and Environmental Sciences, Columbia University, New York, NY 10027, USA

*Correspondence to: jsj@bas.ac.uk

†These authors contributed equally to this work.

‡Present address: Scottish Universities Environmental Research Centre, Rankine Avenue, Scottish Enterprise Technology Park, East Kilbride, G75 0QF, United Kingdom

Abstract: Pine Island Glacier, a major outlet of the West Antarctic Ice Sheet, has been undergoing rapid thinning and retreat for the past two decades. Here we demonstrate, using glacial-geological and geochronological data, that Pine Island Glacier also experienced rapid thinning during the early Holocene, around 8,000 years ago. Cosmogenic ^{10}Be concentrations in glacially-transported rocks show that this thinning was sustained for decades to centuries at an average rate of more than 100 cm yr^{-1}, comparable to contemporary thinning rates. The most likely mechanism was a reduction in ice shelf buttressing. Our findings reveal that Pine Island Glacier has experienced rapid thinning at least once in the past, and that, once set in motion, rapid ice sheet changes in this region can persist for centuries.

Main Text:

Ice mass loss from the Pine Island-Thwaites sector dominates the contemporary contribution to sea level from the West Antarctic Ice Sheet (WAIS) (*1*, *2*). Pine Island Glacier (PIG; Fig. 1A) in particular is currently experiencing significant acceleration, thinning, and retreat (*3*-*6*). This has raised concerns over how much ice will be lost to the ocean before the ice stream stabilises (*5*-*8*). Satellite altimetry measurements show an increase in rates of thinning of ice close to the PIG grounding line from 1.2 m yr^{-1} to 6 m yr^{-1} between 2002 and 2007 (*9*, *4*). In addition, thinning has been detected 150 km upstream of the grounding line (*10*). The pattern of change is best explained by a dynamic response to increased influx of warm water to the cavity under the ice shelf at the glacier front (*11*-*14*). However, the record of change – and our understanding of dynamic changes – over longer timescales of centuries to millennia is still limited. Consequently, there is considerable uncertainty associated with model projections of the future evolution of PIG, and hence rate and timing of future ice loss (*15*). The geological record provides evidence of styles and rates of past ice sheet change that can provide constraints on the

bounds of possible future change (e.g. *16*). In the PIG region, the existing geological record consists largely of marine geological data describing grounding line retreat across the continental shelf (*17-21*). In contrast, little is known about the terrestrial thinning history of PIG (*22*) or how the ice stream evolved through the Holocene to the onset of present-day thinning.

Here we report detailed glacial-geological evidence from the Hudson Mountains (Fig. 1B) for rapid thinning in the PIG system ~8 kyr ago. We studied two nunataks, Mt Moses and Maish Nunatak, located close to the northern margin of PIG within 50 km of its present grounding line (Fig. 1B). An unnamed outlet glacier flows through the Hudson Mountains and feeds into Pine Island Glacier ice shelf (Fig. 1B). In common with many of the ice shelf-tributary glaciers along the Amundsen Sea coast, the outlet glacier is presently thinning rapidly (at a rate of 80-150 cm yr^{-1}; ref. *4*, Fig. S1). At times when the PIG grounding line was beyond Evans Knoll (~45 km seaward of its current position; Fig. 1B), the glacier would have been a tributary to PIG and thus changes in its elevation provide a proxy for past elevation changes of PIG. In this way, the Hudson Mountains provide a 'dipstick' record of PIG thinning during formerly more advanced positions.

Glacial deposits at both sites consist of scattered erratic cobbles and boulders of granitic lithology resting on basaltic bedrock (Fig. S2) (*23*). High-sensitivity ^{10}Be surface exposure dating (*24*) was undertaken on twelve erratics collected between 0 and 142 m above the present ice surface on the two nunataks (Fig. S3). Details of chemical procedures, isotopic data and age calculations are given in (*23*) and Tables S1-S3. All but one sample − whose anomalously-old exposure age (15.8 kyr; Table S2) we attribute to reworking of a previously-exposed cobble − yielded early Holocene ^{10}Be ages, in a narrow time interval from 6.0 ± 0.2 to 8.1 ± 0.3 kyr ago (Fig. 2A, B and C). At Maish Nunatak, exposure ages at all elevations – a range of 100 m − are

indistinguishable. At Mt Moses, the three highest samples yielded exposure ages that are not only indistinguishable over an elevation range of 60 m, but are also indistinguishable from the ages at Maish Nunatak. By 'indistinguishable', we mean that we cannot reject the hypothesis that the scatter of each group of ages around the mean results from measurement uncertainty alone (Table S3) (*23*). We interpret the ages as a record of thinning of the outlet glacier flowing through the Hudson Mountains. Since an ice surface cannot lower infinitely fast, samples at higher elevations must have been exposed for longer than samples at lower elevations. Our observation of indistinguishable exposure ages over a wide elevation range from two nearby nunataks can therefore only be explained by ice sheet thinning that was sufficiently rapid to expose the samples instantaneously with respect to the precision of their exposure ages.

In order to determine the thinning rate at our sites, we fitted separate linear age-elevation models to the data at each nunatak (*23*). Less than 20 km upstream of the modern grounding line, modelled thinning rates that best-fit the exposure age data are 112 and 167 cm yr^{-1} (Fig. 2D). Our uncertainty analysis shows that these cannot be distinguished from contemporary thinning rates (Fig. S1). The early Holocene thinning rates are thus sufficiently high that they imply ice-dynamic change rather than thinning resulting from changes in accumulation and ablation. We infer that previous rapid thinning of the PIG system must have been sustained for several decades, and possibly centuries; our uncertainty analysis indicates 95 % confidence that rapid thinning lasted longer than 25 years (*23*). If we assume that the early Holocene thinning was monotonic, the results of our fitting procedure suggest that, by 7.9 kyr ago, the ice sheet surface at Maish Nunatak had lowered to its present-day elevation and rapid thinning at Mt Moses had ended (Fig. S4). The Maish Nunatak data place some constraint on the onset of contemporary thinning. If present rapid thinning rates have been sustained for several decades, then the ice

surface must have been significantly higher when it started. However, if the ice surface was even a few metres above present for a significant period of the late Holocene, then we would observe erratics with much younger exposure ages at sites adjacent to the modern ice surface than those at higher elevations. Since this is not the case, if the ice surface was above these samples between 7.9 kyr ago and recent decades, it can only have been so for a time comparable to the precision of the exposure ages (i.e. around 100 years). Thus, the most likely scenario consistent with our data is that the ice surface was near its present elevation (or possibly lower, because our observations cannot detect periods of thinner ice) between 7.9 kyr ago and the onset of contemporary thinning.

The high thinning rates determined from our exposure ages imply an ice-dynamic change, since drivers such as a decrease in accumulation rate or increase in atmospheric temperature would produce a slower response. Marine geological and geophysical studies show that the PIG grounding line had retreated to within, but had not stabilised at, 112 km of its present position (core site shown in Fig. 1B and Fig. S5) by 11.7 ± 0.7 kyr ago (*21*), and that a ridge beneath PIG ice shelf (Fig. 1B; Fig. S5) acted as a pinning point for the grounding line prior to the 1970s (*7*). Therefore, potential hypotheses for the mechanism of an early Holocene ice-dynamic change could be: 1) Rapid migration of the PIG grounding line resulting from decoupling from a topographic high, or 2) Reduction in ice shelf buttressing.

First we examine the effect of subglacial topography. This can influence the style of ice stream retreat, for example by providing topographic highs on which pinning can occur (*25*) and by constraining ice stream width (*26, 27*). Whilst the marine geological data constrain retreat of the grounding line landward from the core site to the sub-ice shelf ridge only to sometime between 11.7 ka and the 1970s, they do not preclude that the retreat was associated with inland

thinning at ~8 kyr ago. However, there are no topographic highs seaward of the sub-ice shelf ridge where the grounding line might have been pinned after 11.7 kyr ago (Fig. S5), and from which detachment could have triggered the dynamic thinning inland. Therefore, whilst grounding line retreat may have been associated with the early Holocene thinning, decoupling of the PIG grounding line from a topographic high (hypothesis 1) is unlikely to have been the trigger for it.

Alternatively, thinning may have been the consequence of reduction in buttressing by an ice shelf. Marine sediments have been used to infer the presence of an ice shelf across the middle shelf of the Amundsen Sea prior to ~10.6 ± 0.3 kyr ago (Fig. S5A; *19*). Although the available chronological data cannot resolve when it finally retreated into inner Pine Island Bay, one study suggests it persisted there until ~7 kyr ago (*19*). Glaciers in the Amundsen Sea Embayment and elsewhere in Antarctica have responded to recent ice shelf thinning with acceleration of flow, grounding line retreat, and thinning (*14*). Similarly, subsequent retreat or weakening (e.g. by thinning) of a buttressing ice shelf in Pine Island Bay could have triggered the dynamic thinning in the Hudson Mountains ~ 8 kyr ago. Reduction in ice shelf buttressing would most likely have been initiated by enhanced basal melting in response to inflow of warm Circumpolar Deep Water, as is suggested to account for present thinning (*11*). We favour hypothesis 2 as the most likely mechanism for early Holocene ice-dynamic change, but we cannot rule out more-complicated mechanisms. For example, it is possible that thinning of the outlet glacier may be related to its separation from PIG.

These results have implications for understanding how the Pine Island-Thwaites sector of the WAIS is likely to evolve in coming decades to centuries. The knowledge that PIG has previously undergone sustained dynamic thinning, followed by relative stabilisation over several

millennia prior to the onset of contemporary thinning, suggests that the PIG system can respond quickly to environmental change by abrupt, discontinuous and stepwise retreat. Continued thinning may lead to an even more dramatic response if a dynamic threshold, such as a critical ice shelf thickness or ice flow rate, is exceeded. In addition, the rate and magnitude of early Holocene thinning is consistent with model-based estimates of future PIG thinning sustained over the coming century (*28, 29*), a timescale over which the magnitude of sea level rise most concerns policymakers. In a wider context, the pattern of abrupt past thinning of PIG contrasts with evidence for slower and steadier Holocene deglaciation of other regions of the WAIS (*16, 30*), hinting that a significant part of any WAIS contribution to sea level rise in the early Holocene may have come from its Amundsen Sea sector.

The data presented here demonstrate that thinning of PIG at a rate comparable to that over the past two decades is rare but not unprecedented in the Holocene. Moreover, in contrast to previous glacial-geological work in Antarctica which has provided average thinning rates only over millennial timescales, our data are precise enough to show that rapid thinning of PIG was sustained for at least 25 years, and most likely for much longer. In summary, these data provide a long-term context for contemporary thinning of PIG, suggesting that ongoing ocean-driven melting of PIG ice shelf can result in continued rapid thinning and grounding line retreat for several more decades or even centuries.

References and Notes:

1. M. A. King, R. J. Bingham, P. Moore, P. L. Whitehouse, M. J. Bentley, G. A. Milne, Lower satellite-gravimetry estimates of Antarctic sea-level contribution. *Nature* **491**, 586-589 (2012).

2. A. Shepherd *et al.*, A Reconciled Estimate of Ice-Sheet Mass Balance. *Science* **338**, 1183-1189 (2012).

3. E. Rignot, Changes in West Antarctic ice stream dynamics observed with ALOS PALSAR data. *Geophys. Res. Lett.* **35**, L12505 (2008).

4. H. D. Pritchard, R. J. Arthern, D. G. Vaughan, L. A. Edwards, Extensive dynamic thinning on the margins of the Greenland and Antarctic ice sheets. *Nature* **461**, 971-975 (2009).

5. D. Wingham, D. W. Wallis, A. Shepherd, Spatial and temporal evolution of Pine Island Glacier thinning, 1995–2006. *Geophys. Res. Lett.* **36**, L17501 (2009).

6. J. W. Park, N. Gourmelen, A. Shepherd, S. W. Kim, D. G. Vaughan, D. J. Wingham, Sustained retreat of the Pine Island Glacier. *Geophys. Res. Lett*. **40**, 2137-2142 (2013).

7. A. Jenkins, P. Dutrieux, S. S. Jacobs, S. D. McPhail, J.R. Perrett, Observations beneath Pine Island Glacier in West Antarctica and implications for its retreat. *Nat. Geosci.* **3**, 468-472 (2010).

8. I. Joughin, R. B. Alley, Stability of the West Antarctic ice sheet in a warming world. *Nat. Geosci.* **4**, 506-513 (2011).

9. R. Thomas *et al.*, Accelerated sea-level rise from West Antarctica. *Science* **306**, 255-258 (2004).

10. A. Shepherd, D. J. Wingham, J. A. D. Mansley, H. J. F. Corr, Inland thinning of Pine Island Glacier, West Antarctica. *Science* **291**, 862-864 (2001).

11. S. S. Jacobs, A. Jenkins, C. F. Giulivi, P. Dutrieux, Stronger ocean circulation and increased melting under Pine Island Glacier ice shelf. *Nat. Geosci.* **4**, 519-522 (2011).

12. A. J. Payne, A. Vieli, A. Shepherd, D. J. Wingham, E. Rignot, Recent dramatic thinning of largest West-Antarctic ice stream triggered by oceans. *Geophys. Res. Lett.* **31**, L23401 (2004).

13. A. Shepherd, D. Wingham, E. Rignot, Warm ocean is eroding west Antarctic ice sheet. *Geophys. Res. Lett.* **31**, L23402 (2004).

14. H. D. Pritchard, S. R. M. Ligtenberg, H. A. Fricker, D. G. Vaughan, M. R. van den Broeke, L. Padman, Antarctic ice-sheet loss driven by basal melting of ice shelves. *Nature* **484**, 502-505 (2012).

15. Intergovernmental Panel on Climate Change, in *Climate Change 2007: The Physical Science Basis. Contribution of Working Group I to the Fourth Assessment Report of the Intergovernmental Panel on Climate Change,* S. Solomon, *et al.*, Eds. (Cambridge Univ. Press, Cambridge, 2007).

16. J. O. Stone *et al.*, Holocene deglaciation of Marie Byrd Land, West Antarctica. *Science* **299**, 99-102 (2003).

17. A. L. Lowe, J. B. Anderson, Reconstruction of the West Antarctic ice sheet in Pine Island Bay during the Last Glacial Maximum and its subsequent retreat history. *Quaternary Sci. Rev.* **21**, 1879-1897 (2002).

18. A. G. C. Graham *et al.*, Flow and retreat of the Late Quaternary Pine Island-Thwaites palaeo-ice stream, West Antarctica. *J. Geophys. Res.* **115**, F03025 (2010).

19. A. E. Kirshner, J. B. Anderson, M. Jakobsson, M. O'Regan, W. Majewski, F. O. Nitsche, Post-LGM deglaciation in Pine Island Bay, West Antarctica. *Quaternary Sci. Rev.* **38**, 11-26 (2012).

20. M. Jakobsson *et al.*, Ice sheet retreat dynamics inferred from glacial morphology of the central Pine Island Bay Trough, West Antarctica. *Quaternary Sci. Rev.* **38**, 1-10 (2012).

21. C.-D. Hillenbrand *et al.*, Grounding-line retreat of the West Antarctic Ice Sheet from inner Pine Island Bay. *Geology* **41**, 35-38 (2013).

22. J. S. Johnson, M. J. Bentley, K. Gohl, First exposure ages from the Amundsen Sea Embayment, West Antarctica: The Late Quaternary context for recent thinning of Pine Island, Smith, and Pope Glaciers. *Geology* **36**, 223-226 (2008).

23. Materials and methods are available as Supplementary Materials on *Science* Online.

24. J. M. Schaefer *et al.*, High-Frequency Holocene Glacier Fluctuations in New Zealand Differ from the Northern Signature. *Science* **324**, 622-625 (2009).

25. K. J. Tinto, R. E. Bell, Progressive unpinning of Thwaites Glacier from newly identified offshore ridge: Constraints from aerogravity. *Geophys. Res. Lett.* **38**, L20503 (2011).

26. S. S. R. Jamieson *et al.*, Ice-stream stability on a reverse bed slope. *Nat. Geosci.* **5**, 799-802 (2012).

27. G. H. Gudmundsson, J. Krug, G. Durand, L. Favier, O. Gagliardini, The stability of grounding lines on retrograde slopes. *The Cryosphere* **6**, 1497-1505 (2012).

28. I. Joughin, B. E. Smith, D. M. Holland, Sensitivity of 21st century sea level to ocean-induced thinning of Pine Island Glacier, Antarctica. *Geophys. Res. Lett.* **37**, L20502 (2010).

29. R. M. Gladstone *et al.*, Calibrated prediction of Pine Island Glacier retreat during the 21st and 22nd centuries with a coupled flowline model. *Earth Planet. Sc. Lett.* **333-334**, 191-199 (2012).

30. M. J. Bentley *et al.*, Deglacial history of the West Antarctic Ice Sheet in the Weddell Sea embayment: Constraints on past ice volume change. *Geology* **38**, 411-414 (2010).

31. E. Rignot, J. Mouginot, B. Scheuchl, *MEaSUREs InSAR-Based Antarctica Ice Velocity Map.* (National Snow and Ice Data Center, Boulder, CO, 2011).

32. G. Balco, J. O. Stone, N. A. Lifton, T. J. Dunai, A complete and easily accessible means of calculating surface exposure ages or erosion rates from ^{10}Be and ^{26}Al measurements. *Quat. Geochronol.* **3**, 174-195 (2008).

33. A. E. Putnam *et al.*, In situ cosmogenic ^{10}Be production-rate calibration from the Southern Alps, New Zealand. *Quat. Geochronol.* **5**, 392-409 (2010).

34. G. Balco, J. Briner, R. C. Finkel, J. A. Rayburn, J. C. Ridge, J. M. Schaefer, Regional beryllium-10 production rate calibration for late-glacial northeastern North America. *Quat. Geochronol.* **4**, 93-107 (2009).

35. D. Lal, Cosmic ray labeling of erosion surfaces: in situ nuclide production rates and erosion models. *Earth Planet. Sc. Lett.* **104**, 424-439 (1991).

36. J. O. Stone, Air pressure and cosmogenic isotope productions. *J. Geophys. Res.* **105 (B10)**, 23753-23759 (2000).

37. K. Nishiizumi *et al.*, Cosmic ray production rates of ^{26}Al and ^{10}Be in quartz from glacially polished rocks. *J. Geophys. Res.* **94**, 17907-17915 (1989).

38. R. J. Arthern, D. P. Winebrenner, D. G. Vaughan, Antarctic snow accumulation mapped using polarization of 4.3-cm wavelength microwave emission. *J. Geophys. Res.* **111**, D06107 (2006).

39. P. Fretwell *et al*., Bedmap2: improved ice bed, surface and thickness datasets for Antarctica. *The Cryosphere* **7**, 375-393 (2013).

40. F. O. Nitsche, S. S. Jacobs, R. D. Larter, K. Gohl, Bathymetry of the Amundsen Sea continental shelf: Implications for geology, oceanography, and glaciology. *Geochem. Geophy. Geosy.* **8**, Q10009 (2007).

41. F. O. Nitsche *et al.*, Paleo ice flow and subglacial meltwater dynamics in Pine Island Bay, West Antarctica. *The Cryosphere* **7**, 249-262 (2013).

Supplementary Materials:

Materials and Methods

Figures S1-S5

Tables S1-S3

References (*32-41*)

Acknowledgments: The data presented here are archived in the Supplementary Materials. The project was conceived and developed by M. J. Bentley and R. D. Larter. Fieldwork and sampling were planned and undertaken by M. J. Bentley, J. A. Smith and J. S. Johnson. K. Gohl led the cruise (RV *Polarstern* Expedition ANT-XXVI/3). J. S. Johnson processed the samples and interpreted the data with direction from J. M. Schaefer, and analyses were performed by R. C. Finkel and D. H. Rood. G. Balco developed the Monte Carlo simulations for Fig. 2 and Fig. S4. M. J. Bentley and J. S. Johnson wrote the first draft and all authors contributed to the interpretation and writing of the paper.

This work forms part of the British Antarctic Survey programme ‘Polar Science for Planet Earth’, funded by the Natural Environment Research Council, and was made possible by a Marie Tharp Fellowship in Earth, Environmental, and Ocean Sciences at Columbia University Earth Institute/Lamont-Doherty Earth Observatory, awarded to J. S. Johnson. The fieldwork was supported by the research programme PACES, Topic 3 ‘Lessons from the Past’ of the Alfred Wegener Institute.

Fig. 1. Location of study area. (A) Map of the Amundsen Sea Embayment, showing location of the study area. The grounded ice sheet is shown in dark grey and ice shelves in light grey. The inset shows the location within Antarctica, and the box shows the area covered by (B). **(B)** Map of Pine Island Bay, showing flow velocities (*31*) of Pine Island Glacier and the unnamed outlet glacier flowing through the Hudson Mountains, overlaid on LIMA imagery (greyscale). Contours are in metres. The grounding line is represented by the solid black line, and the crest of the sub-ice shelf ridge (*7*) as a dashed white line. The yellow circle represents a marine sediment core site, PS75/214-1, that constrains grounding line retreat (prior to 11.7 ± 0.7 kyr ago) from Pine Island Bay (*21*).

Fig. 2. Thinning history of the Pine Island Glacier system. (A) and (B) ^{10}Be exposure ages of erratics from Mt Moses and Maish Nunatak relative to the local ice surface. Error bars show 1-sigma measurement uncertainties. Dark lines are linear age-elevation relationships that best fit the exposure age data, and the bundles of lighter lines show age-elevation relationships generated by the Monte Carlo uncertainty analysis (*23*). **(C)** Relationship between ^{10}Be exposure ages from both nunataks. Inset shows representative thinning rates on same axes. One sample from Maish Nunatak with an anomalously-old age (15.8 kyr) is not shown because its age likely reflects prior cosmic ray exposure (e.g. *16*). **(D)** Uncertainty distributions for thinning rates for each nunatak, derived from Monte Carlo simulations. Dashed lines are best-fit thinning rates. Histogram bins are logarithmically-spaced for clarity. 95 % of the Monte Carlo results fell between 8-590 cm yr^{-1} for the period of rapid thinning at Mt Moses, and between 13-550 cm yr^{-1} for thinning at Maish Nunatak. For all panels, the uncertainty distributions do not include systematic uncertainty on ^{10}Be production rate; errors in estimating production rate would act to shift the entire array of ages equally, without changing the relationship between them.

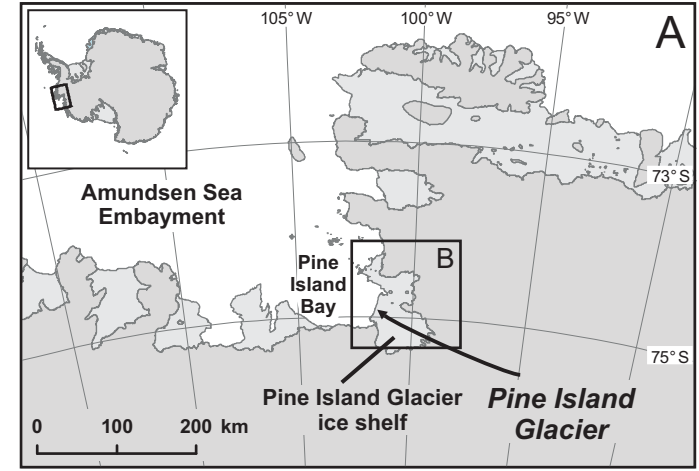
A
105° W
100° W
95° W
73° S
75° S
Amundsen Sea
Embayment
Pine
Island
Bay
B
Pine Island Glacier
ice shelf
Pine Island
Glacier
0
100
200 km

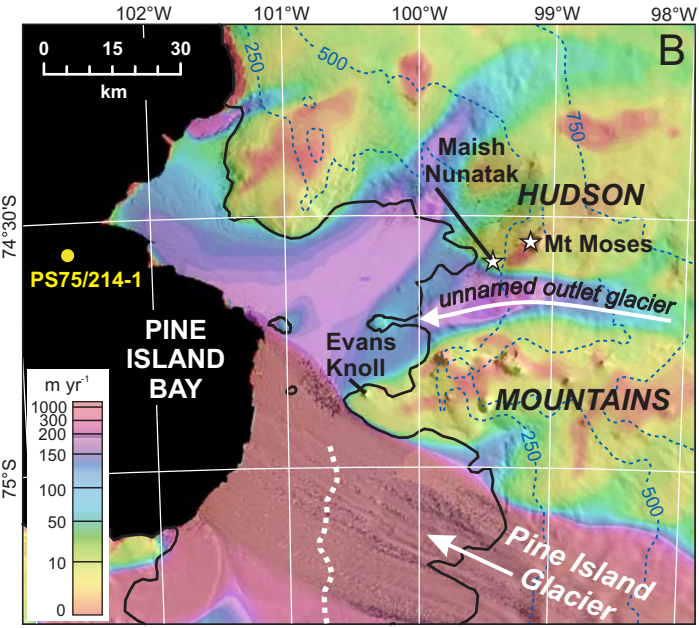
B
102°W
101°W
100°W
99°W
98°W
74°30'S
75°S
0
15
30
km
250
500
750
Maish
Nunatak
HUDSON
MOUNTAINS
Mt Moses
PS75/214-1
unnamed outlet glacier
PINE
ISLAND
BAY
Evans
Knoll
m yr-1
1000
300
200
150
100
50
10
0
Pine Island
Glacier

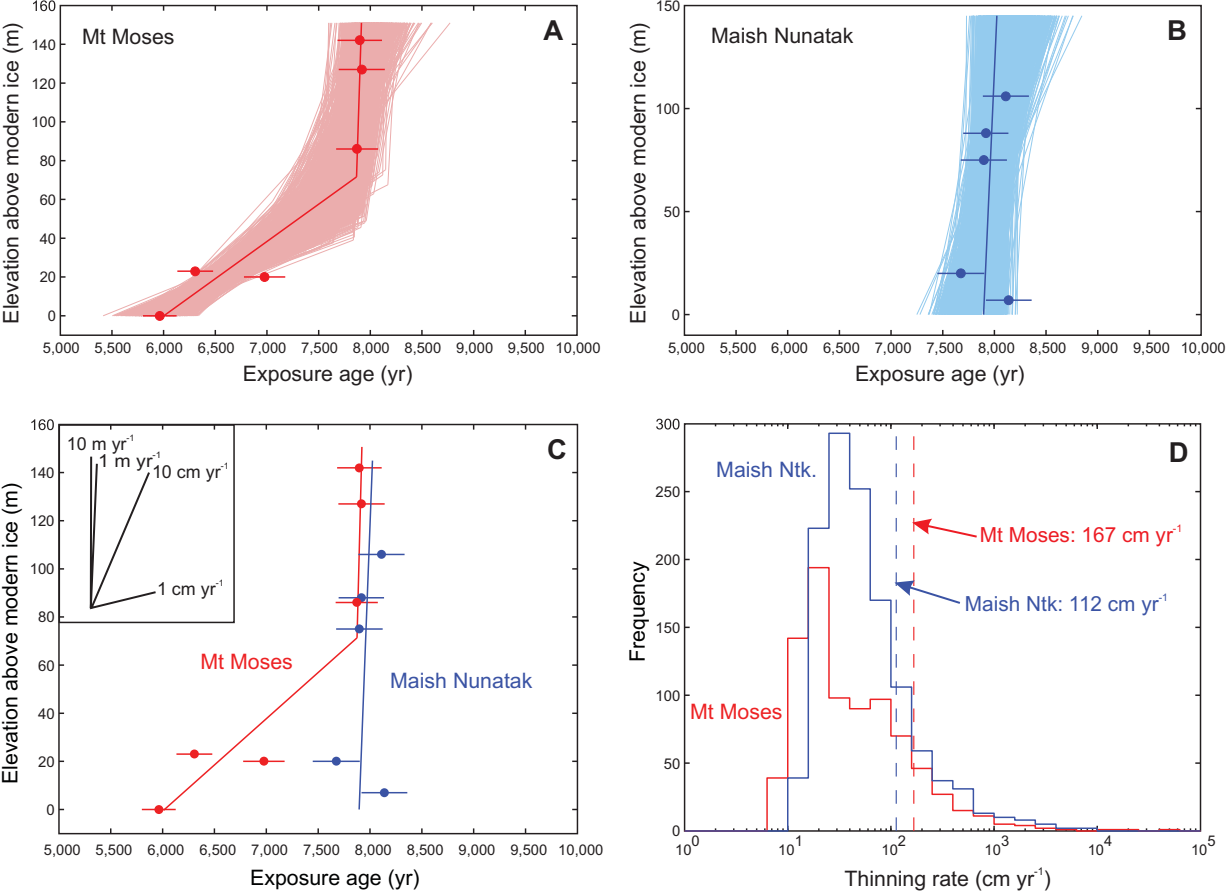
A
Mt Moses
Elevation above modern ice (m)
Exposure age (yr)
B
Maish Nunatak
Elevation above modern ice (m)
Exposure age (yr)
C
10 m yr-1
1 m yr-1
10 cm yr-1
1 cm yr-1
Mt Moses
Maish Nunatak
Elevation above modern ice (m)
Exposure age (yr)
D
Maish Ntk.
Mt Moses: 167 cm yr-1
Maish Ntk: 112 cm yr-1
Mt Moses
Frequency
Thinning rate (cm yr-1)

Supplementary Materials for

Rapid thinning of Pine Island Glacier in the early Holocene

J. S. Johnson, M. J. Bentley, J. A. Smith, R. C. Finkel, D. H. Rood, K. Gohl, G. Balco, R. D. Larter, J. M. Schaefer

correspondence to: jsj@bas.ac.uk

This PDF file includes:

Materials and Methods
Supplementary Text
Figs. S1 to S5

Other Supplementary Materials for this manuscript includes the following:

Tables S1 to S3

Materials and Methods

Samples were collected from the Hudson Mountains during a field campaign undertaken in 2010 using helicopter support from the German research ship *Polarstern* (cruise ANT-XXVI/3). Latitude, longitude and altitude measurements were obtained using a hand-held Garmin GPS and helicopter altimeter, and calibrated to known elevations. Topographic shielding measurements were made using an abney level. Samples were processed at Lamont-Doherty Earth Observatory (LDEO) cosmogenic nuclide laboratory (http://www.ldeo.columbia.edu/res/pi/tcn) according to procedures developed for high-sensitivity ^{10}Be exposure dating (*24*). All analytical details are given in Table S1. Process blanks containing ^{9}Be carrier that were treated identically to the samples yielded levels of ^{10}Be of 10366 ± 2036 to 16368 ± 2302 atoms, which is ~0.2-1.8 % of the ^{10}Be concentration in samples of several 100,000 at g^{-1} ^{10}Be (Table S1). Analysis of ^{10}Be/^{9}Be ratios was undertaken by the Center for Accelerator Mass Spectrometry, Lawrence Livermore National Laboratory, USA. Sample ^{10}Be/^{9}Be ratios were measured relative to the 07KNSTD3110 standard, which has a ^{10}Be/^{9}Be ratio of 2.85×10^{-12}. Those ratios were corrected for background ^{10}Be/^{9}Be using procedural blanks, and for boron interference (^{10}B is an interfering isobar of ^{10}Be).

We used the CRONUS-Earth online calculator (*32*) to calculate exposure ages from the ^{10}Be measurements. The topographic shielding factor was calculated using the online geometric shielding calculator, v. 1.1 (*32*). We assumed zero erosion and a quartz density of 2.7 g cm^{-3}, and used the Antarctic pressure curve for the input file. We consider the ^{10}Be production rate based on a calibration site in New Zealand (P_{NZ}; *33*) as the most appropriate for our samples because that calibration site (44 ºS) is closer to the Hudson Mountains (74-75 ºS) than any of those on which the global (P_{GLOBAL}; *32*) or northeast North America (P_{NENA}; *34*) production rates are based (57 ºN-9 ºS and 42-69 ºN, respectively). Using P_{NENA} instead does not affect our interpretations. The CRONUS-Earth online calculator has a developmental version which incorporates P_{NZ} (available at: http://hess.ess.washington.edu/math/al_be_v22/Age_input_NZ_calib.html), and is based on age calculation version 2.1, muon calculation version 2.1 and constant version 2.2 (*32*). We used this for calculating our ^{10}Be exposure ages. ^{10}Be ages from our sites in Antarctica must be calculated by extrapolating production rates for ^{10}Be (by spallation) from the New Zealand calibration site using one of five published scaling schemes. We chose to report exposure ages based on the 'Lm' scaling (*35-37*). Using any of the other published scaling schemes (*32*) changes the exposure ages by up to 4.6 % (Table S2). We have not applied a snow cover correction to our exposure ages. However, assuming a snow cover of 140 cm (*38*) for 6 months of every year (with a snow density of 0.25 g cm^{-3}, cosmic ray attenuation length of 165 g cm^{-3}, and average cobble height of 20 cm), the reported exposure ages change by only 8.3 % (thus making the early Holocene thinning period slightly earlier, from 6.5 ± 0.2 to 8.8 ± 0.3 ka). We did not include an uncertainty in the sample elevations; typical precision of elevation measurements is < 5 m. None of these uncertainties alter our interpretations of thinning rate. We used the chi-squared statistic (χ^2) to evaluate the hypothesis that the scatter in exposure ages recording rapid thinning ~8 kyr ago results from measurement uncertainty alone. Given only measurement uncertainty in the exposure ages (i.e. not common uncertainty from production rate estimates): 1) for samples at Maish Nunatak, $\chi^2 = 2.80$ for 4 degrees of

freedom (d.o.f.), and $p = 0.59$ (where p is the probability of occurrence of χ^2 equal to or greater than observed given normally-distributed data with stated uncertainties), 2) for the upper three samples at Mt Moses, $\chi^2 = 0.024$ for 2 d.o.f. ($p = 0.99$), and 3) for these samples together, $\chi^2 = 2.95$ for 7 d.o.f. ($p = 0.89$).

To estimate thinning rates implied by the exposure age data set, we first used an error-weighted least-squares regression to fit a linear age-elevation history to the Maish Nunatak data (Fig. 2B) and a 2-segment, piecewise-linear age-elevation history to the Mt Moses data (Fig. 2A). Note that because analytical uncertainties in all exposure ages are similar, error-weighted and non-error-weighted regressions yield indistinguishable results. To estimate uncertainties in these thinning rate estimates, we conducted a 2000-iteration Monte Carlo simulation in which we randomly sampled sets of exposure ages from normal distributions defined by the exposure ages and their analytical ("internal") uncertainties (Table S2), and repeated the regression analysis for each random sample. We discarded as unphysical any iteration that yielded a zero or negative age-elevation slope, i.e., a thinning rate greater than or equal to infinity. Fig. 2 (A and B) shows the set of age-elevation histories generated by the Monte Carlo simulation. The resulting uncertainty distributions for thinning rates during the period of rapid thinning are highly skewed (Fig. 2D), so cannot be accurately described by a mean and standard deviation. For the period of rapid thinning at Mt Moses, 68 % and 95 % of the Monte Carlo results fell between 10-100 cm yr^{-1} and 8-590 cm yr^{-1}, respectively. At Maish Nunatak, 68 % and 95 % of results fell between 18-90 cm yr^{-1} and 13-550 cm yr^{-1}, respectively. To estimate the minimum duration of rapid thinning consistent with the exposure-age data, we observe that 95 % of Monte Carlo estimates for thinning rates are below 450 cm yr^{-1} at Maish Nunatak and below 385 cm yr^{-1} at Mt Moses. The 100 m elevation range of the Maish Nunatak data shows that a minimum of 100 m of thinning took place, so these rates imply greater than 95 % confidence that thinning was sustained for at least 22 or 26 years, respectively. The assumption of a two-segment, piecewise-linear thinning history at Mt Moses implies that the break in slope represents the cessation of rapid thinning; given this assumption, the Monte Carlo results provide estimated uncertainty distributions for the timing of this event (Fig. S4A). Likewise, they provide an uncertainty estimate for the time the ice surface reached its present elevation at Maish Nunatak (Fig. S4B).

Supplementary Text

Site Descriptions and Sampling Strategy

Twelve samples for surface exposure dating were collected from Mt Moses and Maish Nunatak in the Hudson Mountains, to establish a detailed record of ice sheet surface profile change through time. Mt Moses is an eroded volcano, and Maish Nunatak, 9 km to the WSW of Mt Moses, is probably a small parasitic cone. The bedrock of Mt Moses is dominated by basaltic pillow lavas and hyaloclastite breccias, whilst Maish Nunatak consists of basaltic lavas. The regional ice flow direction is south-westerly at these sites (Fig. S2A). The NW flank of Mt Moses and NNW-SSE trending ridges at Maish Nunatak (Figs. S2A and S3A) are strewn with numerous large quartz-bearing (granite and syenite) erratics resting on basaltic bedrock/talus. No basement is exposed at

either nunatak, suggesting that these erratics were plucked and transported at the base of an expanded ice sheet.

Sampling for surface exposure dating was focused on the lowermost ~140 m in order to accurately constrain the most recent glacial history. The erratics sampled varied from small cobbles (~15 cm long axis) through to large (~1.5 m^3) boulders (Fig. S3). With the exception of MTM-06 and JF-04, which were sub-sampled in the field, all other erratics were collected whole. The lowermost flank of Mt Moses has an adjacent wind scoop and so the lowest sample (MTM-06) was collected at, or very slightly below, the regional ice surface (Fig. S2). Wind scoops are maintained by wind-scouring around local topography. The physiography of the flank of Mt Moses does not change significantly higher up, and there is significant exposed relief at elevations above our sample sites; for these reasons it is reasonable to assume that the wind scoop was present even when the ice sheet was >140 m thicker. Thus, sample altitudes are plotted in Fig. 2 relative to the present-day local ice surface (where the ice intersects the rock).

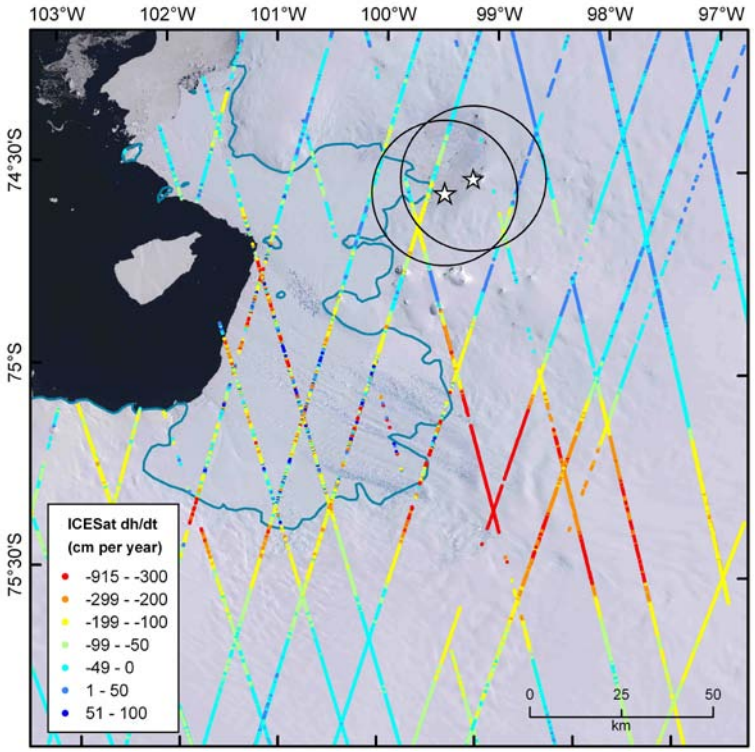

Fig. S1.

Contemporary ice sheet thinning rates in study area. Firn-corrected ICESat data [after (*4*)], showing thinning rates (dh/ht) from 2003-2007 across Pine Island Glacier and the Hudson Mountains. Within a 20 km radius (indicated by circles) of Mt Moses and Maish Nunatak (stars), the average thinning rate is 90 ± 57 cm yr^{-1}. The underlying image is from LIMA (Landsat Image Mosaic of Antarctica), and the present grounding line position is represented by the solid blue line.

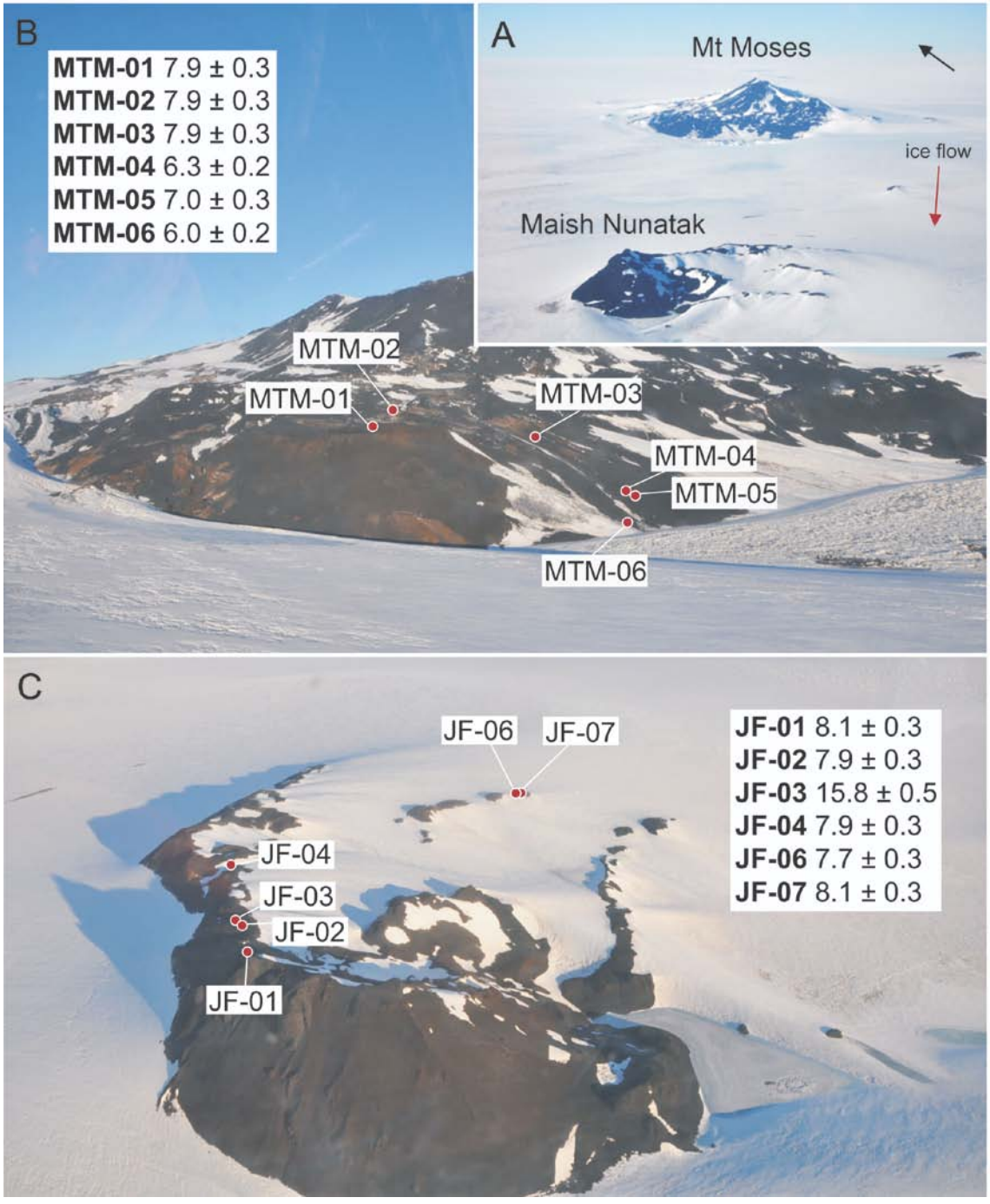

Fig. S2

Locations of erratics sampled for cosmogenic isotope analysis. (A) Oblique aerial photograph of Mt Moses (summit 749 m asl) and Maish Nunatak (310 m asl). The unnamed outlet flows past the flanks of Mt Moses and Maish Nunatak, indicated by red arrow. **(B) and (C)** Photographs of south-west side of Mt Moses, and north-west side of Maish Nunatak, respectively. Sample locations are shown as red dots, and ^{10}Be exposure ages are shown in kyr.

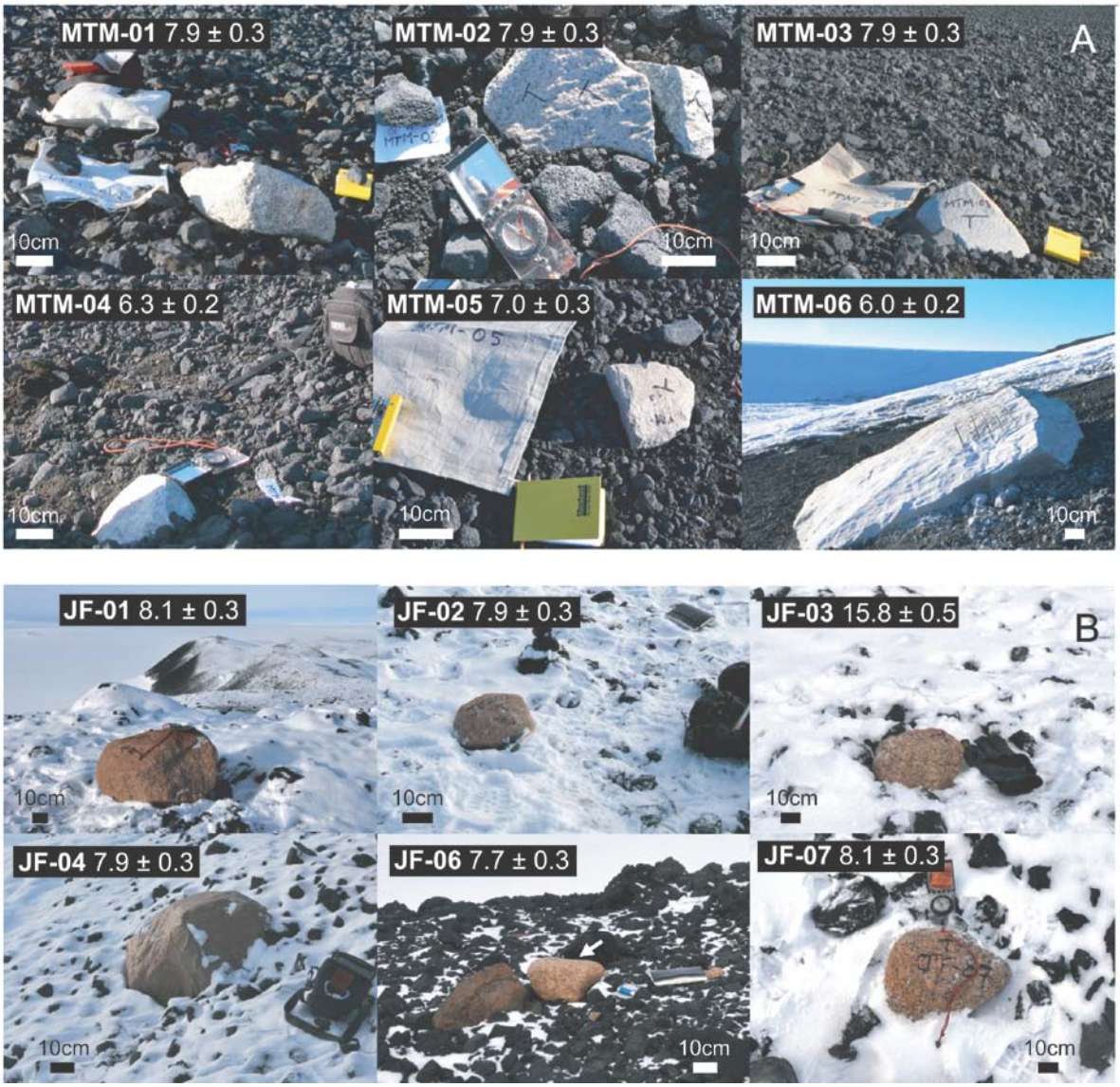

Fig. S3

Photographs of erratics sampled for cosmogenic isotope analysis. (A) and (B) Photographs of samples collected from Mt Moses and Maish Nunatak, respectively. ^{10}Be exposure ages (kyr) are also shown.

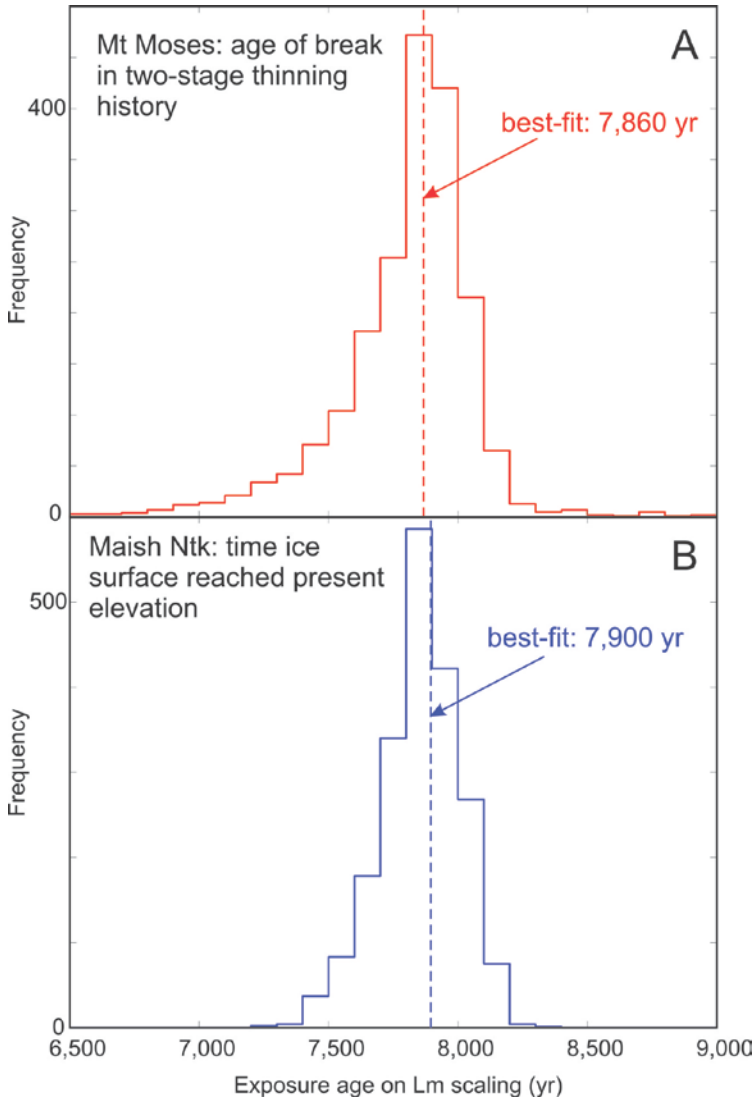

Fig. S4

Timing of thinning at Mt Moses and Maish Nunatak. (A) Best-fitting value (dashed line) and the uncertainty distribution derived from the Monte Carlo simulation (histogram) for the timing of the break in slope in the model thinning history at Mt Moses, which provides an estimate of the time thinning ceased. **(B)** Best-fitting value (dashed line) and uncertainty distribution derived from the Monte Carlo simulation (histogram) for the time the ice surface reached its present elevation at Maish Nunatak. The uncertainty estimates shown do not include the systematic uncertainty on ^{10}Be production rate.

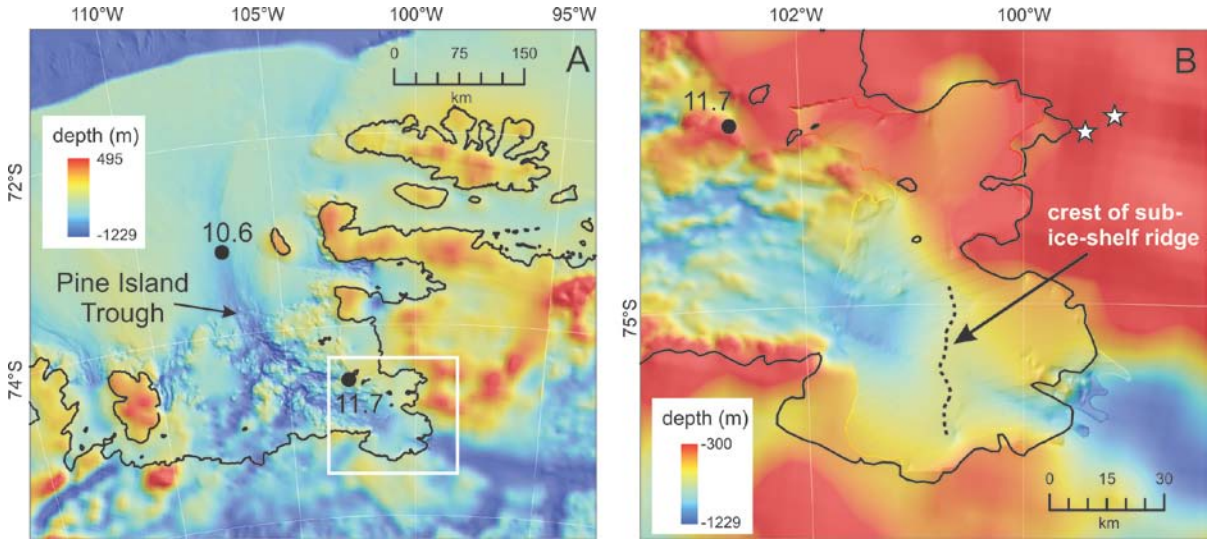

Fig. S5

Bedrock topography in the Amundsen Sea and Pine Island Bay. (A) Bedrock topography in the Amundsen Sea Embayment (*7, 39-41*), showing present location of Pine Island Trough and grounding line (black line). Box denotes location of Fig. S5B. **(B)** Bedrock topography for inner Pine Island Bay (*7*), showing location of study sites (stars). In both panels, filled black circles with ages (kyr) are core sites (*19, 21*) mentioned in the text. The ages of these cores differ in what they represent: the 10.6 kyr age from site KC19 (*19*) is not a minimum age for grounding line retreat like 11.7 kyr (*21*), but instead reflects the time after which an ice shelf was absent from the middle shelf of the Amundsen Sea.

Table S1 (separate file)
Sample details and ^{10}Be data.

Table S2 (separate file)
Comparison of ^{10}Be exposure ages calculated with the available production rates and scaling schemes.

Table S3 (separate file)
Chi-squared (χ^2) scores for sets of exposure ages recording rapid thinning.